Measurements of sediment pickup rate over dune-covered bed

Emadzadeh, Adel; Cheng, Nian-Sheng

2015

Emadzadeh, A., & Cheng, N.-S. Measurements of sediment pickup rate over dune-covered bed. Environmental Fluid Mechanics, in press.

https://hdl.handle.net/10356/79373

https://doi.org/10.1007/s10652-015-9416-1

Measurements of sediment pickup rate over dune-covered bed

Adel Emadzadeh[1] Nian-Sheng Cheng[2]

Abstract Laboratory experiments were conducted to measure sediment pickup rate over two-dimensional fixed dunes. Measurements were performed over both stoss and lee sides of the dune with sediments of D_{50} = 0.23, 0.44 and 0.86 mm. Flow velocity and turbulence were also measured by using an Acoustic Doppler Velocimeter (ADV). By analysing the experimental data, an empirical sediment pickup function based on depth-averaged flow parameters was proposed to estimate the pickup rate over the dune.

Keywords Dune; Open channel flow; Pickup rate; Sediment transport; Turbulence

1 Introduction

Sediment pickup from a channel bed serves as an essential component in the understanding of bedload and suspended load transport. In the formulation of his bedload function, Einstein [13] considered both pickup and deposition processes using a probabilistic approach. In the study of suspended load transport, the pickup rate can be used to specify the upward sediment flux as a boundary condition [42] and therefore is critical to predict the distribution of suspended sediment over the flow depth [41]. In addition, entrainment or pickup rate serves as a substantial component in quantifying the source term of mass conservation equations [6,47]. Due to the poor understanding of sediment transport near the bed, sediment motion predicted by a numerical model may differ significantly from experimental data [35,46]. Many studies have been conducted to investigate details of bed particle movements, such as

[1] Adel Emadzadeh
School of Civil and Environmental Engineering, Nanyang Technological Univ., Nanyang Ave., Singapore, 639798. Tel.: +65-97573000, E-mail: aemadzadeh@ntu.edu.sg

[2] Nian-Sheng Cheng
School of Civil and Environmental Engineering, Nanyang Technological Univ., Nanyang Ave., Singapore, 639798. Tel.: +65-67906936, E-mail: cnscheng@ntu.edu.sg

step length [24,34], and saltation height and velocity (See [8] for a recent review). However due to the complex nature of turbulence structure and fluid-particle interactions involved in the entrainment and deposition processes, theoretical solutions to sediment pickup remain unresolved and the current knowledge is derived mainly from experimental efforts.

LeFeuvre et al. [17] appeared the first to investigate the pickup rate in a horizontal smooth pipe. Van Rijn [39] conducted pickup rate measurements in open channel flows and measured the pickup rate with a sediment injector from the bed. Nielsen [30] developed a pickup function based on Van Rijn's [39] formula for modelling sediment transport in coastal boundary layers. Damgaard et al. [11] and Dey and Debnath [12] studied the effect of bed slope on pickup rate in closed conduits. It is noted that all those studies have been carried out over flat beds or under uniform flow condition. In comparison, very limited information is available on the pickup rate in nonuniform flows or over bedforms such as dunes. As a typical bedform in natural rivers and coastal waters, dunes exerts considerable influence on sediment entrainment and flow resistance. Therefore knowledge of pickup rate over the dune is crucial to further understand sediment transport mechanics.

Being closely related to pickup function, the near bed concentration of suspended sediment has been investigated over ripples [35] and over developing and fixed dunes [25,26,43,45] . However, only McLean et al. [18], Miwa et al. [22] and Miwa and Daido [21] focused on sediment entrainment over two dimensional fixed dunes. McLean et al. [18] carried out measurements of turbulence and sediment transport rate over fixed two dimensional bedforms with height δ = 4 cm, wave length λ = 80 cm and lee side angle $\alpha = 30^o$. They replaced one of the concrete dune models with erodible sands formed in approximately the same shape as the fixed dunes. Sediment transport rate was then calculated by measuring the change in the bed topography using acoustic profilers. Their results showed that over the dune, the local boundary shear stress is poorly correlated with the local transport rate. Furthermore they mentioned that the statistics of the near-bed turbulence does not scale with the local shear velocity u_*. Therefore, they suggested that classical sediment transport formulas such as that suggested by Meyer-Peter and Muller [20] which use the mean bed shear stress cannot predict the sediment transport

rate over the dune. Similar observation was also presented by Nelson et al. [27]. Miwa et al. [22] and Miwa and Daido [21] conducted sediment transport and pickup rate measurements over a fixed two dimensional dune (δ = 2 cm, λ = 40 cm and $\alpha = 45^o$). They intended to formulate a mean step length function based on turbulence intensity and particle Reynolds number to estimate the pickup rate over the dune. They measured the sediment pickup rate based on the weight of the particles entrained form the surface of rectangular openings designed at eleven sections on the stoss side of the dune model. The openings measured 3 cm in the streamwise and 10 cm in the spanwise direction. Application of the sediment pickup rate function introduced by Miwa and Daido [21] requires estimation of the lift and drag force coefficients, the shear velocity and the critical Shields number τ_{*_c}, which are all difficult to define over a dune. A recent study that is relevant is due to Mohtar and Munro [23] who examined the sediment threshold over a dune in presence of oscillating-grid turbulence. In their experiments with no mean flow, incipient grain motion was only induced as a result of turbulent fluctuations. They studied the threshold criteria in terms of a modified Shields parameter. However, when compared with the original Shields diagram, the predicted values of initiation of motion were twice greater than those predicted from the Shields diagram.

More recently Naqshband et al. [25,26] conducted simultaneous velocity and sediment concentration measurements over mobile migrating sand dunes in equilibrium using Acoustic Concentration and velocity profiler (ACVP). Their results show that upward sediment fluxes or sediment pickup occurred over the entire dune with large peaks on the stoss side of the dune downstream of the flow reattachment point. The large pickup rates result from the shear layer vortices that impact the dune bed and generate turbulent sediment bursts.

Current approaches to predicting the sediment transport over the surface of a dune are largely based on the methods developed for steady, uniform flows. Under uniform flow conditions, the fluid turbulence that gives rise to instantaneous hydrodynamic forces resulting in sediment transport is scaled with the shear velocity. Therefore, sediment transport in particular the bedload transport rate can be effectively characterized by the shear velocity. However, experimental measurements and theoretical

considerations reveal that over the bedforms where the flow is not uniform and the local turbulence varies significantly with bed position, near-bed turbulence is not necessarily correlated with the local mean flow characteristics and thus sediment entrainment may not be characterized by the local bed shear stress or shear velocity [18,23,27,28,33].

In the present study, experimental effort was made to examine how the sediment pickup rate varies over a typical dune for a given flow condition. Three sizes of sediments were employed for the measurements of pickup rate and flow velocity in open channel flows with fixed dunes.

2 Experimental setup

The experiments were conducted in a tilting-recirculating flume with glass walls and a steel bed which was 14 m long, 0.6 m wide and 0.6 m deep. Water was recirculated by a pump and the discharge was measured using an electromagnetic flow meter with $3\times10^{-4}\ m^3s^{-1}$ precision in the flow return pipe. Water level was measured with a precision of 1 mm by a moving point gage throughout the flume. The fixed dune bed consisted of a train of 15 identical two-dimensional dunes formed from aluminium plate which covered almost the entire channel bed. The use of fixed dunes allowed long sampling time and precise positioning of sensors. Moreover, by roughening the surface of the dunes, it is possible to achieve quasi-uniform flows over the periodic boundary [18].

The pickup rate and relevant flow velocity measurements were carried out on the 10th dune (the distance from the flume entrance x = 9 - 9.8 m) so that the turbulent flow can be considered to be fully developed. The initial reach (1 m long) from the flume entrance was covered by a layer (4 cm thick) of coarse gravel with size D_{50} = 3.2 cm to accelerate the development of the boundary layer. The dunes were identical in shape and size to those used in earlier experimental studies by Nelson and Smith [29], Nelson et al. [27], McLean et al. [18] and McLean et al. [19], with wave length λ = 80 cm, dune height δ = 4 cm and lee side angel $\alpha = 30^o$. The curvature of the stoss side of the dune followed a half-cosine curve, providing a reasonable approximation of a natural bedform shape (Fig. 1). Bridge and Best [5] and Bennett and Best [2] suggested the following ratios between the dune height

δ, wavelength λ and the flow depth H ($\lambda/H \approx 4-5$, $\lambda/\delta \approx 15-75$, $H/\delta \approx 2-9$) which is in agreement with the dune size and wavelength used in the current study. The results reported by Nelson and Smith [29] and Nelson et al. [27] for a similar setup showed that the equilibrium condition was reached around the fifth dune.

The flume was equipped with a sediment supply system attached to the channel bottom through a rectangular opening, which measured 1.5 cm in the streamwise direction and 10 cm in the spanwise direction and located at a section 9 m downstream from the entrance. The sediment supply system was connected to the openings on the model dune as illustrated in Fig. 1. Pickup rates were measured at 8 sections over the dune, each standing 10 cm apart from its neighbour. While pickup rate was measured in one section, the openings in the other sections were closed with lids. The dune model in the test section and the lids were designed in such a way that when all the lids were put in place, the dune model was identical to all the rest roughened with the same sediment particles.

In each run, the same sediment as in the supply system was pasted on the dune models throughout the flume. A thin mist of adhesive glue was sprayed on the surface of the aluminum dunes and a single layer of sediment particles were evenly distributed on the dunes by a device similar to a salt dispenser. After the surface got dry, another thin layer of adhesive was sprayed over the surface to ensure that the particles were effectively fixed on the dunes. The layer of adhesive glue used in the experiments was very thin compared to the sediment size and it could not affect the bed roughness. Further information related to the experimental setup is given in Emadzadeh [14].

In the sediment injecting system, sediment particles were pushed upward at a constant rate with a piston driven by an electrical motor. The lifting speed of the piston and therefore the sediment supply rate was adjusted by the control box. With the aid of a gear box, the upward speed of the piston could be reduced to 0.2 mm/min to facilitate low pickup rate measurements. Three sets of uniform sediments with median size D_{50} = 0.23, 0.44 and 0.86 mm (Table 1) were used in the experiments. Pickup rate E was measured based on the total volume of entrained sediment, which were calculated from the area

of the injector opening and the piston displacement measured by a mechanical dial gage with the precision of 0.01 mm,

$$E = \frac{V}{AT} \tag{1}$$

where $V = V_T(1-\varepsilon)$ is the sediment volume; V_T is the bulk volume of sediment entrained; ε is the sediment porosity ; A is the bed observation area and T is the time duration for pickup measurements.

Prior to each experiment the flume was filled with water to a certain depth and the sediment injector was loaded with sediment particles. The sediment was first submerged in water in a separate glass container and then stirred in order to release the air. Then it was poured inside the injector with a funnel beneath the water surface. The particles were briefly stirred inside the slot once more before the commencement of the experiment to ensure that loosely packed sediments could not affect the pickup rate measurements. For each sediment size, pickup rate measurements were carried out with three flow discharges and the flow depth $H \approx$ 20 cm measured from the crest of dunes to the water surface on a fixed slope $S =$ 0.0005.

In each run the electrical motor was turned on and the lifting speed of the piston was adjusted visually to avoid formation of a hump or a pit over the observation area. A hump may form over the injection slot if the sediment supply rate was higher than the pickup rate and on the contrary, there would be a pit in the observation area if the supply rate was lower than the flow entrainment capacity. When the sediment injection rate was set accurately, only a single layer of moving particles was observed over and downstream the injector opening. The upward movement of the piston was relatively slow compared to the fall velocity of the sediment particles, and therefore this movement had no considerable effect on the lift force and thus the pickup rate.

Once the sediment injection and entrainment rate reached equilibrium, piston displacement and time were recorded. Each run was repeated at least five times in the same condition to make sure that statistically reliable entrainment rate data were recorded. The results were considered acceptable only

when the variation among them was less than 15 % from the average. The standard deviation of the measurements was computed and then normalized by their mean as an indicator of the variation in the pickup rate measurements. The normalized standard deviation had an average of 7 % for all the experiments and a maximum of 15 % for the very large pickup rates for which the sediment particles loaded in the lift were entrained in less than a minute.

Flow velocity and turbulence measurements were carried out using a 3D down-looking Acoustic Doppler Velocimeter (ADV) manufactured by Nortek (http://www.nortek-as.com/). The instrument has four acoustic sensors working with 10 MHz acoustic frequency and a cylindrical sampling volume 6 mm in diameter and 7 mm in length located 5 cm below the acoustic transmitter. The ADV was positioned at the centerline of the flume right above the injection slot and velocity measurements were carried out prior to or after the pickup measurements. For each velocity profile 18-20 points were sampled at a rate of 50 Hz for 3 minutes.

There are some difficulties and unreliability of measurements reported associated with ADVs especially in highly turbulent zones and in the vicinity of the bed where the lower bound of the sampling volume interferes with the bed [15,37]. To eliminate these adverse effects, measurements were started from $z =$ 5 mm from the bed. To enhance quality of flow measurements, an air bubble generating system was designed and positioned on the trough of the upstream dune preceding the test section. This system consisted of a mesh made from 0.2 mm stainless steel wire, which was connected to a direct current to generate tiny bubbles. Application of the artificial seeding significantly enhanced the signal-to-noise ratio (SNR) and correlation (COR) of the measurements. The SNR value that should be at least higher than 15 dB for accurate turbulence measurements [36] was above 50 dB in the current measurements and COR ranged between 60-70% which was lower than the recommended value (70 %) by the manufacturer but natural for highly turbulent flows [37]. The raw ADV data were then processed using software WinADV [44].

3 Results

3.1 Mean flow velocity and turbulence

Vertical profiles of the mean flow velocity in the streamwise direction u are illustrated in Fig. 2 for all the measuring sections. Section 1 (X = 6.5 cm) was located in the separation zone with negative velocity close to the bed. Positive near-bed velocities at section 2 (X =16.5 cm) indicate that flow reattachment occurred upstream of this section which is approximately 4 times the dune height δ = 4 cm. This result is consistent with previous studies [3,4,18]. Over the stoss side, accelerating flow is induced by the change in the bed topography increasing the near-bed flow velocity from sections 2-7. The sudden expansion in the lee side affects the velocity profile in section 8, where negative flow velocities are observed near the bed. The variations in the mean flow velocity in the streamwise direction highlight the flow acceleration on the stoss side from the point of reattachment to the crest and flow deceleration afterwards.

Fig. 3 illustrates the Reynolds shear stress distribution $\tau_{xz} / \rho = -\overline{u'w'}$ over the dune where u' and w' are the instantaneous velocity fluctuations in the streamwise and vertical directions. This figure shows that the Reynolds shear stress has the maximum value in the separation zone and decreases over the dune surface from sections 2-7. The Reynolds shear stress distribution measured in the present study is consistent with previous results [3,18].

Under uniform flow conditions, the bed shear stress can be estimated either from the logarithmic velocity profile or the linear distribution of the Reynolds shear stress. For flows over dunes, Bennett and Best [3] extended the spatial average of the Reynolds shear stress profile to the mean bed elevation to estimate the mean bed shear stress. McLean et al. [18] and Nelson et al. [28] used $\tau_{xz} = -\rho\overline{u'w'}$ at Z =5 mm to estimate the bed shear stress. In the current study the bed shear stress was estimated from the maximum in the τ_{xz} profile, and it is denoted as τ_{max} in the next section.

In this study, turbulence kinetic energy is taken as a measure of turbulence intensity. It is defined as $k = \left(\overline{u'^2} + \overline{v'^2} + \overline{w'^2} \right) / 2$, which quantifies the energy extracted from the mean flow by the motion of turbulent eddies [16]. The variation of k in the streamwise direction is illustrated in Fig. 4. Similar to the τ_{xz} distribution (Fig. 3), the vertical distribution of k achieves its maximum values within the separation zone and reduces gradually towards downstream. The k distribution measured in the current study is similar to previous measurements (e.g. Venditti and Bennett [43]). All velocity and turbulence measurements are provided as an Online Resource accompanying this article.

Figs. 2-4 show that downstream the reattachment point (sections 2-7) the mean flow velocity increases in the streamwise direction but the Reynolds shear stress τ_{xz} and turbulence kinetic energy k decrease. It is noted that the pickup rate increases with increasing near-bed mean flow velocity and also turbulence kinetic energy. Therefore, for flows over a dune, the mean flow velocity and turbulence kinetic energy appear to have opposite effects on the pickup rate. In other words, the entrainment capacity would increase due to the mean flow and decrease due to the turbulence. This is discussed in detail next.

3.2 Pickup rate

In this section, the pickup rate measurements in the different sections over the dune are presented in terms of both near-bed and depth-averaged flow parameters. Shown in the next section are possible relations between these parameters and the pickup rate. Figs. 5(a)-(c) illustrate the variation of the flow parameters and the measured pickup rate along the dune model for sediment sizes D_{50} = 0.23, 0.44 and 0.86 mm. For each sediment size, three flow conditions were selected with the depth $H \approx$ 20 cm and different discharges (see Table 2). In these figures τ_{max} and k_{max} are the maximum values observed in τ_{xz} and k profiles which occur close to the bed. In the streamwise direction, both τ_{max} and k_{max} show their maximum values in the separation zone and decrease monotonically towards the dune crest

(sections 1-7). At section 8, there is a sharp increase in these values due to recirculation of the flow within the wake region.

Contrary to uniform flow condition where approaches are available to link the near-bed flow parameters to the depth-averaged ones, nonuniform flows cause the link not resolved due to non-linear distribution of the Reynolds shear stress and the failure of the logarithmic law especially in the wake region. Therefore in this section the variation of both depth-averaged and near-bed parameters are studied over the dune and the effect of these parameters on the pickup rate is investigated in the next section.

Variations of the depth-averaged values of mean flow velocity U and turbulence kinetic energy K are presented for each run in Fig. 5. The depth-averaged flow velocity U shows the same trend as u as presented in Fig. 2. Change in the bed elevation induces acceleration in the flow field and therefore U increases from section 1 to section 7. However downstream the dune crest, the flow decelerates due to the sudden expansion of the cross section and therefore lower U values are observed at section 8.

The depth-averaged turbulence kinetic energy, on the other hand, has an opposite trend in comparison to the U variation. Since the flow separation is the source of turbulence in the wake region, K decreases from its maximum value at section 1 to minimum at section 7. However, at section 8 there is a sudden increase in the values of K as it was also observed in τ_{max} and k_{max}.

Sediment pickup rate measurements plotted in Fig. 5 shows that the entrainment rate increases from section 1 in the wake zone to its maximum value at section 7 close to the dune crest, which is consistent with the measurements of McLean et al. [18] and Miwa et al. [22]. At section 1, due to the recirculating flow, particle movements were against the mean flow direction and the entrained particles moved towards the trough and the upstream dune crest. As a result, the entrained particles would return to the injector opening from time to time. The pickup rates presented in Table 2 for section 1 are based

on the overall volume of the entrained particles in a long period of time containing both entrainment and deposition. At section 8 no particle movement was observed over the injector opening.

Fig. 5 shows that the peak in the pickup rate values in all experiments occurs near the dune crest. The effect of the flow acceleration on the stoss side of the dune is so strong that it overwhelms the effect of turbulence and forces the particles to entrain at higher rates in spite of the negative bed slope.

3.3 Regression analysis

In this section a dimensional analysis is first performed to identify important dimensionless parameters that affect the sediment pickup rate over the surface of a dune. Regression analysis is then applied to find empirical relations between different independent parameters and pickup rate.

To simplify the analysis, the following assumptions are made: (1) the flow is steady and fully turbulent; (2) the channel is wide so that the flow is considered two-dimensional and (3) the sediment particles are of uniform size. Sediment pickup rate E depends on variables shown as follows

$$E = f\left(\tau, k_b, k_s, H, \delta, g, \rho, \rho_s, \nu\right) \tag{2}$$

where τ is the mean bed shear stress, k_b is the near-bed turbulence kinetic energy, k_s is the equivalent bed roughness, g is the gravitational acceleration, ρ is the fluid density, ρ_s is the sediment density and ν is the fluid viscosity.

To estimate the parameters in Eq. (2), it is assumed that the mean bed shear stress τ scales with the maximum of Reynolds shear stress distribution $\tau_{max} = -\rho\overline{(u'w')}_{\max}$. In addition, k_b is taken as the maximum turbulent kinetic energy k_{max}. Since uniform sediments were used in the current study, k_s is estimated as the sediment diameter D in the sense of roughness length scale. By choosing ρ, g, and D as repeating variables, Eq. (2) can be transformed to

$$\frac{E}{\sqrt{gD}} = f\left(\frac{\tau_{\max}}{\Delta gD}, \frac{k_{\max}}{gD}, \frac{H}{D}, \frac{\delta}{D}, D\left(\frac{g}{\nu^2}\right)^{\frac{1}{3}}\right) \tag{3}$$

Since H and δ are constant in all the experiments, H/D and δ/D have negligible effects on the pickup rate. By combining some dimensionless parameters, Eq. (3) can be further expressed as

$$\frac{E}{\sqrt{\Delta gD}} = f\left(\frac{\tau_{\max}}{\Delta gD}, \frac{k_{\max}}{\Delta gD}, D\left(\frac{\Delta g}{\nu^2}\right)^{\frac{1}{3}}\right) \text{ or } E_* = f(\tau_*, k_*, D_*) \tag{4}$$

In Eq. (4), $E_* = E/\sqrt{\Delta gD}$ is the dimensionless pickup rate, $\tau_* = \tau_{\max}/\Delta gD$ is the Shields parameter, $k_* = k_{max}/\Delta gD$ is the dimensionless turbulence kinetic energy and $D_* = D(\Delta g/\nu^2)^{1/3}$ is the dimensionless sediment diameter. In these three parameters, $\Delta(=\rho_s/\rho - 1)$ and g are combined in a product form to quantify the reduced effect of gravity for submerged sediment particles [7].

Regression analysis was then performed to examine the effect of the independent near-bed parameters τ_*, k_* and D_* on the dimensionless pickup rate E_*. It was assumed that pickup function in Eq. (4) can be expressed in a multiplicative power form as

$$E_* = e^{a_1}\tau_*^{a_2}k_*^{a_3}D_*^{a_4} \tag{5}$$

where $a_1 - a_4$ are constants. The multiplicative power form which was also used by Van Rijn [39] and Dey and Debnath [12] facilitates linear regression analysis of the logarithmically transformed variables in Eq. (5). Using regression analysis, the constants are calibrated with the data and Eq. (5) is expressed as

$$E_* = 8.34\times10^{-8}\tau_*^{-6.1}k_*^{6.2}D_*^{0.1} \tag{6}$$

It should be noted that in performing regression analysis using Eq. (5) the data collected at section 8 with E = 0 were not included in the analysis. Computed and measured dimensionless pickup rates are compared in terms of average relative error

$$Err = \frac{1}{n}\sum \frac{\left|E_{*cal} - E_{*data}\right|}{E_{*data}} \times 100\% \tag{7}$$

where n is the total number of data points and cal and $data$ subscripts denote the calculated and measured E_*. The calculated error is Err = 60.1 % and the computed and measured values of E_* are compared in Fig. 6(a).

Under uniform flow conditions, the shear velocity u_* is a function of U, k_s, H and ν in the form of $U/u_* = f(H/k_s, u_* k_s/\nu)$. In nonuniform flows such as the flow over the dune, the Reynolds shear stress τ_{xz} distribution is not linear and the logarithmic law is not applicable in the wake zone and also the developing boundary layer on the stoss side of the dune. Therefore it is difficult to estimate the shear velocity u_* and therefore apply the Shields parameter to predict the entrainment rate. Alternatively the near-bed flow parameters such as τ and k_b could be replaced with the depth-averaged parameters U and K. Therefore Eq. (2) is rewritten as

$$E = f\left(U, K, D, g, \rho, \rho_s, \nu\right) \tag{8}$$

By performing dimensional analysis, Eq. (8) is expressed as

$$\frac{E}{\sqrt{\Delta g D}} = f\left(\frac{U}{\sqrt{\Delta g D}}, \frac{K}{\Delta g D}, D\left(\frac{\Delta g}{\nu^2}\right)^{\frac{1}{3}}\right) \text{ or } E_* = f(Fr_*, K_*, D_*) \tag{9}$$

In Eq. (9), Fr_* is the densimetric Froude number which is widely used in the prediction of scour depth [1,10,31,32]. Performing regression analysis using the data from sections 1-7, and calibrating the exponents in Eq. (9) results in

$$E_* = 2.81\times10^{-13} K_*^{-0.8} Fr_*^{8} D_*^{2.4} \tag{10}$$

Fig. 3(b) shows the comparison between the measured and predicted dimensionless pickup rate. The error associate with the prediction of Eq. (10) is Err = 19.7 % which is about 40 % smaller than the predictions of Eq. (6). From the comparison between Figs. 6(a) and 6(b) it follows that the depth-averaged parameters are more reasonable for the prediction of the pickup rate over the dunes.

4 Comparisons with previous studies

The experiments in the present study were conducted over a channel bed covered only with fixed dunes. The experimental setup facilitates pickup rate measurements, but the data collected would differ from those measured in the presence of mobile beds, at which both erosion and deposition occur simultaneously. Recently, sediment pickup over mobile dunes was studied by Naqshband et al. [26], who measured sediment fluxes in the bedload layer used an ACVP. Their results show that sediment pickup occurred over the entire dune with large peaks observed on the stoss side of the dune, which result from the shear layer vortices that impact the dune bed and generate turbulent sediment bursts. In spite of the fixed dunes used for the experiments, the results obtained in the present study are found to be qualitatively consistent with Naqshband et al.'s [26] observations. This is understandable by noting that the celerity of a mobile dune is only a few percent of the average flow velocity [9].

Next, an attempt is made to compare the data obtained with Van Rijn's [39] pickup function, which was developed for open channel flows. The following procedure is applied. First, both flow depth and pickup rate are averaged over the stoss side of the dune. Then, the equivalent bed roughness height is estimated as [38]

$$k_s = 1.1\delta(1 - e^{-25\delta/\lambda}) \tag{11}$$

and the shear velocity is calculated as

$$u_* = \frac{U}{2.5\ln(H/k_s) + 6.23} \tag{12}$$

where U is the depth-averaged flow velocity that was estimated as Q/(BH) here. Next, the effective shear velocity is calculated as [40],

$$u_*' = \frac{\sqrt{g}\,U}{18\log[(12H)/(3D_{90})]} \tag{13}$$

and thus the corresponding Shields number τ_*'. Finally, the pickup rate is calculated,

$$E = 0.00033 D_*^{0.3} \sqrt{\Delta g D} \left(\frac{\tau_*' - \tau_{*c}}{\tau_{*c}} \right)^{1.5} \tag{14}$$

The above calculations provide spatial averaged values, and their comparisons with the measurements averaged over the dune are shown in Fig. 7. It is interesting to note that all the calculations are consistently larger than the corresponding measurements, and the ratio is close to 3.1 times. The significant difference may be partially explained by the fact that in the presence of fixed dunes, energy dissipates mainly due to form drag rather than sediment entrainment, which yields reduced pickup rates. The comparison also implies that in a numerical model, applying van Rijn's pickup function to dune-covered sediment beds may result in erosion rates that are higher than measurements.

5 Conclusions

An experimental study was carried out to investigate the sediment pickup rate over a fixed two-dimensional dune. Variations of the mean flow velocity, bed shear stress, turbulence kinetic energy and pickup rate were measured at 8 sections over the stoss and lee sides of the dune. The results show that the turbulence kinetic energy decreased in the streamwise direction from the point of reattachment

downstream the separation zone towards the dune crest. However the mean flow velocity increased in the streamwise direction due to the acceleration imposed by the change in the bed elevation. Pickup rate measurements show that the accelerating flow has dominating effects on the pickup rate, which results in the maximum entrainment close to the dune crest where the turbulence kinetic energy is at its minimum.

Dimensional analyses were performed by using both near-bed and depth-averaged flow parameters. Two sets of regression analyses yield the relation involving independent near-bed dimensionless parameters, $E_* = f(\tau_*, k_*, D_*)$ and also that involving the depth-averaged parameters, $E_* = f(Fr_*, K_*, D_*)$. The results are in favour of the depth-averaged flow parameters which predict the pickup rate more satisfactory than the near-bed flow variables. The comparison with previous studies shows that over a fixed dune, the average pickup rates predicted by applying the van Rijn's pickup function are about 3.1 times higher than the measurements.

Notations

A	Pickup observation area (m^2)
$a_1, a_2, ...$	Constants
B	Channel width (m)
D	Sediment diameter (m)
D_*	Dimensionless particle diameter
E	Sediment pickup rate (m/s)
E_*	Dimensionless pickup rate
Err	Average of the relative error (%)
f	Function
Fr_*	Densimetric Froude number (--)
g	Gravitational acceleration (ms^{-2})
H	Flow depth (m)
K	Depth-averaged k (m^2s^{-2})
K_*	Dimensionless depth-averaged turbulence kinetic energy K
k	Turbulence kinetic energy (m^2s^{-2})
k_s	Equivalent sand roughness (m)
k_*	Dimensionless maximum Turbulence kinetic energy k_{max}
n	Coefficient
Q	Flow discharge (m^3s^{-1})
S	Bed slope
T	Time period for pickup measurements (s)
U	Depth-averaged u (m/s)
u, v, w	Streamwise, spanwise and vertical velocity (m/s)
u_*	Shear velocity (m/s)
u_*'	Effective shear velocity (m/s)
V_T	Total volume of sediment (m^3)
x	Streamwise distance (m)
z	Vertical distance from the bed (m)
α	Dune lee side angle (^{o})
δ	Dune height (m)
ε	Sediment porosity
λ	Dune wave length (m)
ν	Kinematic viscosity (m^2s^{-1})
ρ	Fluid density (kgm^{-3})
ρ_s	Sediment density (kgm^{-3})
σ_g	Geometric standard deviation $\sigma_g = \sqrt{D_{84}/D_{16}}$
τ	Mean bed shear stress (Nm^{-2})
τ_*	Shields parameter

τ_*'	Effective Shields parameter
τ_{*_c}	Critical Shields number
τ_{xz}	Bed shear stress (Nm^{-2})
Δ	Specific submerged density

References

1. Aguirre-Pe J, Olivero ML, Moncada AT (2003) Particle densimetric Froude number for estimating sediment transport. J Hydraul Eng 129 (6):428-437. doi:10.1061/(asce)0733-9429(2003)129:6(428)

2. Bennett SJ, Best JL (1995) Mean flow and turbulence structure over fixed, 2-dimensional dunes - implications for sediment transport and bedform stability. Sedimentology 42 (3):491-513. doi:10.1111/j.1365-3091.1995.tb00386.x

3. Bennett SJ, Best JL (1995) Mean flow and turbulence structure over fixed, 2-dimensional dunes - implications for sediment transport and bedform stability (Vol 42, pg 491, 1995). Sedimentology 42 (5):830-830. doi:10.1111/j.1365-3091.1995.tb00386.x

4. Best J (2005) The fluid dynamics of river dunes: A review and some future research directions. J Geophys Res Earth Surface 110 (F4):F04S02. doi:10.1029/2004JF000218

5. Bridge JS, Best JL (1988) Flow, sediment transport and bedform dynamics over the transition from dunes to upper-stage plane beds - implications for the formation of laminae. Sedimentology 35 (5):753-763. doi:10.1111/j.1365-3091.1988.tb01249.x

6. Cao ZX (1997) Turbulent bursting-based sediment entrainment function. J Hydraul Eng 123 (3):233-236. doi:10.1061/(asce)0733-9429(1997)123:3(233)

7. Cheng NS (2011) Application of Incomplete Self-Similarity Argument for Predicting Bed-Material Load Discharge. J Hydraul Eng 137 (9):921-931. doi:10.1061/(ASCE)HY.1943-7900.0000375

8. Cheng NS, Emadzadeh A (2014) Average Velocity of Solitary Coarse Grain in Flows over Smooth and Rough Beds. J Hydraul Eng 140 (6):04014015. doi:10.1061/(ASCE)HY.1943-7900.0000875

9. Chien N, Wan Z (1999) Mechanics of sediment transport. ASCE Press. Reston, Virginia.

10. Chiew YM, Lim S (1996) Local Scour by a Deeply Submerged Horizontal Circular Jet. J Hydraul Eng 122 (9):529-532. doi:doi:10.1061/(ASCE)0733-9429(1996)122:9(529)

11. Damgaard JS, Whitehouse RJS, Soulsby RL (1997) Bed-load sediment transport on steep longitudinal slopes. J Hydraul Eng 123 (12):1130-1138. doi:10.1061/(ASCE)0733-9429(1997)123:12(1130)

12. Dey S, Debnath K (2001) Sediment pickup on streamwise sloping beds. J Irrig Drainage Eng 127 (1):39-43. doi:10.1061/(ASCE)0733-9437(2001)127:1(39)

13. Einstein HA (1950) The bed-load function for sediment transportation in open channel flows. Tech Bull 1026, Soil Conserv Serv, US Dep Agric, Washington, DC Tech. Bull. 1026

14. Emadzadeh A (2014) Experimental investigation of turbulence effects on sediment pickup rate in open channel flows. Nanyang Technological University, Singapore

15. Finelli CM, Hart DD, Fonseca DM (1999) Evaluating the spatial resolution of an acoustic Doppler velocimeter and the consequences for measuring near-bed flows. Limnology and Oceanography 44 (7):1793-1801. doi:10.4319/lo.1999.44.7.1793

16. Kline SJ, Reynolds WC, Schraub FA, Runstadler PW (1967) The structure of turbulent boundary layers. J Fluid Mech 30 (04):741-773. doi:doi:10.1017/S0022112067001740

17. LeFeuvre AR, Altinbilek HD, Carstens MR (1970) Sediment-Pickup Function. J Hydr Div 96 (10):2051-2063

18. McLean SR, Nelson JM, Wolfe SR (1994) Turbulence structure over 2-dimensional bed forms - implications for sediment transport. J Geophys Res Oceans 99 (C6):12729-12747. doi:10.1029/94JC00571

19. McLean SR, Wolfe SR, Nelson JM (1999) Predicting boundary shear stress and sediment transport over bed forms. J Hydraul Eng 125 (7):725-736. doi:10.1061/(ASCE)0733-9429(1999)125:7(725)

20. Meyer-Peter E, Muller R Formulas for bed-load transport. In: Proceedings of the 2nd Meeting Stockholm, Sweden., 1948. Int. Assoc. Hydraulic Structures Res., pp 39-64

21. Miwa H, Daido A Step length formula of bed-load sediment and its application to dune-bed. In: The 7th Int. Conf. on Hydroscience and Engineering (ICHE-2006), Philadelphia,USA, 2006.

22. Miwa H, Daido A, Kato I Sediment Pick-up rate Formula and its Application to Dune-beds. In, 2000.

23. Mohtar W, Munro RJ (2013) Threshold criteria for incipient sediment motion on an inclined bedform in the presence of oscillating-grid turbulence. Phys Fluids 25 (1). doi:10.1063/1.4774341

24. Nakagawa H, Tsujimoto T (1980) Sand bed instability due to bed load motion. J Hydr Div 106 (12):2029-2051

25. Naqshband S, Ribberink JS, Hulscher SJMH (2014) Using Both Free Surface Effect and Sediment Transport Mode Parameters in Defining the Morphology of River Dunes and Their Evolution to Upper Stage Plane Beds. J Hydraul Eng 140 (6):06014010. doi:doi:10.1061/(ASCE)HY.1943-7900.0000873

26. Naqshband S, Ribberink JS, Hurther D, Hulscher SJMH (2014) Bed load and suspended load contributions to migrating sand dunes in equilibrium. J Geophys Res Earth Surface 119 (5):2013JF003043. doi:10.1002/2013JF003043

27. Nelson JM, McLean SR, Wolfe SR (1993) Mean flow and turbulence fields over 2-dimensional bed forms. Water Resour Res 29 (12):3935-3953. doi:10.1029/93WR01932

28. Nelson JM, Shreve RL, McLean SR, Drake TG (1995) Role of near-bed turbulence structure in bed-load transport and bed form mechanics. Water Resour Res 31 (8):2071-2086. doi:10.1029/95wr00976

29. Nelson JM, Smith JD (1989) Mechanics of flow over ripples and dunes. J Geophys Res Oceans 94 (C6):8146-8162. doi:10.1029/JC094iC06p08146

30. Nielsen P (1992) Coastal bottom boundary layers and sediment transport. World Scientific, Singapore

31. Oliveto G, Hager WH (2005) Further results to time-dependent local scour at bridge elements. J Hydraul Eng 131 (2):97-105. doi:10.1061/(asce)0733-9429(2005)131:2(97)

32. Rajaratnam N (1981) Erosion by plane turbulent jets. J Hydraul Res V 19 (N 4):277-305. doi:10.1080/00221688109499508

33. Raudkivi AJ (1966) Bed forms in alluvial channels. J Fluid Mech 26 (3):507-514. doi:10.1017/S0022112066001356

34. Sekine M, Kikkawa H (1992) Mechanics of Saltating Grains. II. J Hydraul Eng 118 (4):536-558. doi:10.1061/(ASCE)0733-9429(1992)118:4(536)

35. Sleath JFA, Wallbridge S (2002) Pickup from rippled beds in oscillatory flow. J Waterw, Port, Coastal, Ocean Eng 128 (6):228-237. doi:10.1061/(asce)0733-950x(2002)128:6(228)

36. Sontek (1997) Sontek ADV Operation Manual. Firmware Version 4.0. Sontek, San Diego

37. Strom KB, Papanicolaou AN (2007) ADV measurements around a cluster microform in a shallow mountain stream. J Hydraul Eng 133 (12):1379-1389. doi:10.1061/(ASCE)0733-9429(2007)133:12(1379)

38. van Rijn LC (1982) Equivalent roughness of alluvial bed. Journal of the Hydraulics Division 118 (12):1215-1218

39. van Rijn LC (1984) Sediment pick-up functions. J Hydraul Eng 110 (10):1494-1502. doi:10.1061/(ASCE)0733-9429(1984)110:10(1494)

40. van Rijn LC (1984) Sediment Transport, Part I: Bed Load Transport. J Hydraul Eng 110 (10):1431-1456. doi:doi:10.1061/(ASCE)0733-9429(1984)110:10(1431)

41. van Rijn LC (1984) Sediment Transport, Part II: Suspended Load Transport. J Hydraul Eng 110 (11):1613-1641. doi:10.1061/(ASCE)0733-9429(1984)110:11(1613)

42. van Rijn LC (1986) Application of sediment pick-up function. J Hydraul Eng 112 (9):867-874. doi:10.1061/(ASCE)0733-9429(1986)112:9(867)

43. Venditti JG, Bennett SJ (2000) Spectral analysis of turbulent flow and suspended sediment transport over fixed dunes. J Geophys Res Oceans 105 (C9):22035-22047. doi:10.1029/2000JC900094

44. Wahl T (2000) Analyzing ADV Data Using WinADV. Paper presented at the Joint Conference on Water Resource Engineering and Water Resources Planning and Management, Minneapolis, Minnesota, United States,

45. Wren DG, Kuhnle RA (2008) Measurements of coupled fluid and sediment motion over mobile sand dunes in a laboratory flume. Int J Sediment Res 23 (4):329-337. doi:10.1016/S1001-6279(09)60004-4

46. Zedler EA, Street RL (2001) Large-eddy simulation of sediment transport: Currents over ripples. J Hydraul Eng 127 (6):444-452. doi:10.1061/(asce)0733-9429(2001)127:6(444)

47. Zhong DY, Wang GQ, Ding Y (2011) Bed Sediment Entrainment Function Based on Kinetic Theory. J Hydraul Eng 137 (2):222-233. doi:10.1061/(asce)hy.1943-7900.0000299

Table 1 Properties of sediments used in experiments

D_{50} (mm)	D_{16} (mm)	D_{84} (mm)	σ_g	ε	Δ
0.23	0.22	0.27	1.11	0.441	1.65
0.44	0.31	0.53	1.31	0.435	1.65
0.86	0.65	1	1.24	0.406	1.65

Table 2 Experimental data of pickup rate

No.	Section	Q (m^3/s)	H (m)	D (m)	τ_{max} (N/m^2)	k_{max} (m^2/s^2)	U (m/s)	K (m^2/s^2)	E ($m^3/m^2/s$)
1	D1-0.23-1	0.050	0.234	0.00023	2.38	8.78E-03	0.407	2.07E-03	8.26E-06
2	D1-0.23-2	0.050	0.226	0.00023	1.86	7.09E-03	0.416	1.91E-03	7.25E-06
3	D1-0.23-3	0.050	0.218	0.00023	1.23	4.42E-03	0.408	1.73E-03	8.45E-06
4	D1-0.23-4	0.050	0.212	0.00023	0.82	3.42E-03	0.415	1.53E-03	9.43E-06
5	D1-0.23-5	0.050	0.206	0.00023	0.75	2.87E-03	0.426	1.45E-03	1.67E-05
6	D1-0.23-6	0.050	0.202	0.00023	0.57	2.46E-03	0.432	1.37E-03	1.92E-05
7	D1-0.23-7	0.050	0.200	0.00023	0.52	2.30E-03	0.445	1.31E-03	2.26E-05
8	D1-0.23-8	0.050	0.220	0.00023	1.45	5.36E-03	0.402	1.64E-03	0
9	D2-0.23-1	0.056	0.233	0.00023	3.01	1.05E-02	0.451	2.61E-03	1.46E-05
10	D2-0.23-2	0.056	0.225	0.00023	2.60	8.61E-03	0.466	2.44E-03	1.46E-05
11	D2-0.23-3	0.056	0.217	0.00023	1.43	5.50E-03	0.465	1.94E-03	1.68E-05
12	D2-0.23-4	0.056	0.211	0.00023	1.05	4.19E-03	0.476	1.74E-03	2.43E-05
13	D2-0.23-5	0.056	0.205	0.00023	0.89	3.76E-03	0.487	1.65E-03	3.94E-05
14	D2-0.23-6	0.056	0.201	0.00023	0.73	3.20E-03	0.497	1.54E-03	4.32E-05
15	D2-0.23-7	0.056	0.199	0.00023	0.70	2.86E-03	0.504	1.50E-03	4.58E-05
16	D2-0.23-8	0.056	0.219	0.00023	2.23	7.59E-03	0.458	1.72E-03	0
17	D3-0.23-1	0.061	0.233	0.00023	3.38	1.25E-02	0.475	3.22E-03	2.86E-05
18	D3-0.23-2	0.061	0.225	0.00023	3.27	1.11E-02	0.499	2.86E-03	3.32E-05
19	D3-0.23-3	0.061	0.217	0.00023	1.83	6.83E-03	0.514	2.29E-03	4.12E-05
20	D3-0.23-4	0.061	0.211	0.00023	1.38	5.43E-03	0.531	2.08E-03	4.73E-05
21	D3-0.23-5	0.061	0.205	0.00023	1.11	4.58E-03	0.541	1.96E-03	5.20E-05
22	D3-0.23-6	0.061	0.201	0.00023	0.94	4.17E-03	0.551	1.87E-03	6.33E-05
23	D3-0.23-7	0.061	0.199	0.00023	0.83	3.58E-03	0.554	1.82E-03	9.40E-05
24	D3-0.23-8	0.061	0.219	0.00023	3.90	1.35E-02	0.504	2.37E-03	0
25	D1-0.44-1	0.056	0.234	0.00044	3.11	1.08E-02	0.480	2.71E-03	9.55E-06
26	D1-0.44-2	0.056	0.226	0.00044	2.12	8.15E-03	0.453	2.46E-03	1.40E-05
27	D1-0.44-3	0.056	0.218	0.00044	1.53	6.11E-03	0.499	2.23E-03	3.03E-05
28	D1-0.44-4	0.056	0.212	0.00044	0.98	4.09E-03	0.494	1.77E-03	3.86E-05
29	D1-0.44-5	0.056	0.206	0.00044	0.94	3.81E-03	0.516	1.60E-03	4.29E-05
30	D1-0.44-6	0.056	0.202	0.00044	0.73	3.09E-03	0.500	1.61E-03	5.27E-05
31	D1-0.44-7	0.056	0.200	0.00044	0.63	2.86E-03	0.517	1.83E-03	6.19E-05
32	D1-0.44-8	0.056	0.220	0.00044	2.16	7.78E-03	0.456	2.05E-03	0
33	D2-0.44-1	0.061	0.232	0.00044	3.77	1.29E-02	0.496	3.19E-03	1.93E-05
34	D2-0.44-2	0.061	0.224	0.00044	2.23	8.71E-03	0.503	2.78E-03	3.57E-05
35	D2-0.44-3	0.061	0.216	0.00044	1.95	7.19E-03	0.524	2.56E-03	4.23E-05
36	D2-0.44-4	0.061	0.210	0.00044	1.29	5.34E-03	0.549	2.09E-03	6.21E-05
37	D2-0.44-5	0.061	0.204	0.00044	1.11	4.39E-03	0.557	2.02E-03	7.31E-05
38	D2-0.44-6	0.061	0.200	0.00044	0.95	3.94E-03	0.556	1.88E-03	7.72E-05
39	D2-0.44-7	0.061	0.198	0.00044	0.74	3.36E-03	0.564	2.14E-03	1.04E-04
40	D2-0.44-8	0.061	0.218	0.00044	2.70	9.61E-03	0.494	2.51E-03	0
41	D3-0.44-1	0.067	0.231	0.00044	3.86	1.51E-02	0.536	3.72E-03	3.08E-05

42	D3-0.44-2	0.067	0.223	0.00044	2.86	1.03E-02	0.541	3.25E-03	5.31E-05
43	D3-0.44-3	0.067	0.215	0.00044	2.18	8.22E-03	0.562	2.79E-03	7.72E-05
44	D3-0.44-4	0.067	0.209	0.00044	1.57	6.43E-03	0.589	2.51E-03	1.10E-04
45	D3-0.44-5	0.067	0.203	0.00044	1.19	5.14E-03	0.602	2.30E-03	1.09E-04
46	D3-0.44-6	0.067	0.199	0.00044	1.07	4.52E-03	0.606	2.37E-03	1.36E-04
47	D3-0.44-7	0.067	0.197	0.00044	0.94	4.25E-03	0.616	2.37E-03	1.55E-04
48	D3-0.44-8	0.067	0.217	0.00044	3.33	1.25E-02	0.548	2.95E-03	0
49	D1-0.86-1	0.061	0.234	0.00086	3.24	1.14E-02	0.469	2.93E-03	6.53E-06
50	D1-0.86-2	0.061	0.226	0.00086	2.84	1.02E-02	0.483	2.74E-03	1.35E-05
51	D1-0.86-3	0.061	0.218	0.00086	1.95	6.97E-03	0.487	2.69E-03	1.81E-05
52	D1-0.86-4	0.061	0.212	0.00086	1.49	5.66E-03	0.514	2.40E-03	1.93E-05
53	D1-0.86-5	0.061	0.206	0.00086	1.34	4.93E-03	0.535	2.29E-03	2.69E-05
54	D1-0.86-6	0.061	0.202	0.00086	1.12	4.25E-03	0.550	2.23E-03	4.45E-05
55	D1-0.86-7	0.061	0.200	0.00086	0.94	4.41E-03	0.543	2.16E-03	4.97E-05
56	D1-0.86-8	0.061	0.220	0.00086	3.13	1.09E-02	0.501	2.86E-03	0
57	D2-0.86-1	0.067	0.232	0.00086	3.52	1.26E-02	0.519	3.76E-03	1.42E-05
58	D2-0.86-2	0.067	0.224	0.00086	3.36	1.23E-02	0.532	3.56E-03	2.87E-05
59	D2-0.86-3	0.067	0.216	0.00086	2.26	8.45E-03	0.528	3.09E-03	4.05E-05
60	D2-0.86-4	0.067	0.210	0.00086	1.69	6.68E-03	0.564	2.72E-03	4.48E-05
61	D2-0.86-5	0.067	0.204	0.00086	1.51	5.76E-03	0.577	2.60E-03	5.76E-05
62	D2-0.86-6	0.067	0.200	0.00086	1.26	4.99E-03	0.598	2.57E-03	6.83E-05
63	D2-0.86-7	0.067	0.198	0.00086	1.16	4.91E-03	0.589	2.58E-03	9.46E-05
64	D2-0.86-8	0.067	0.218	0.00086	3.96	1.37E-02	0.538	3.35E-03	0
65	D3-0.86-1	0.072	0.231	0.00086	3.79	1.43E-02	0.558	4.01E-03	2.30E-05
66	D3-0.86-2	0.072	0.223	0.00086	4.27	1.50E-02	0.562	3.94E-03	5.00E-05
67	D3-0.86-3	0.072	0.215	0.00086	3.19	1.06E-02	0.582	3.54E-03	5.90E-05
68	D3-0.86-4	0.072	0.209	0.00086	2.08	7.72E-03	0.589	3.00E-03	7.41E-05
69	D3-0.86-5	0.072	0.203	0.00086	1.62	6.34E-03	0.614	2.86E-03	7.85E-05
70	D3-0.86-6	0.072	0.199	0.00086	1.44	5.68E-03	0.641	2.91E-03	9.00E-05
71	D3-0.86-7	0.072	0.197	0.00086	1.34	5.42E-03	0.633	2.87E-03	1.31E-04
72	D3-0.86-8	0.072	0.217	0.00086	4.34	1.52E-02	0.580	3.18E-03	0

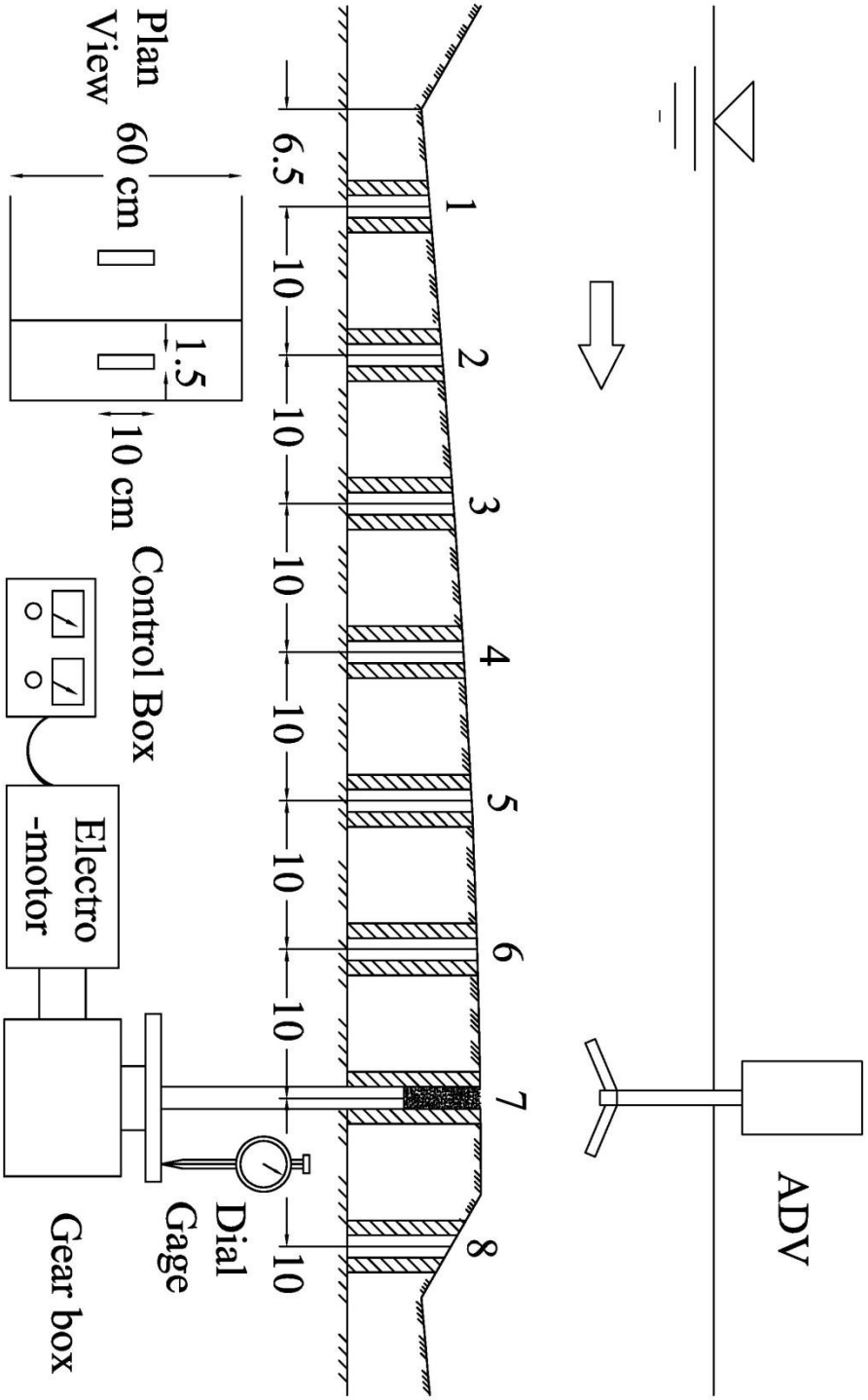

Fig. 1 Experimental setup (not to scale)

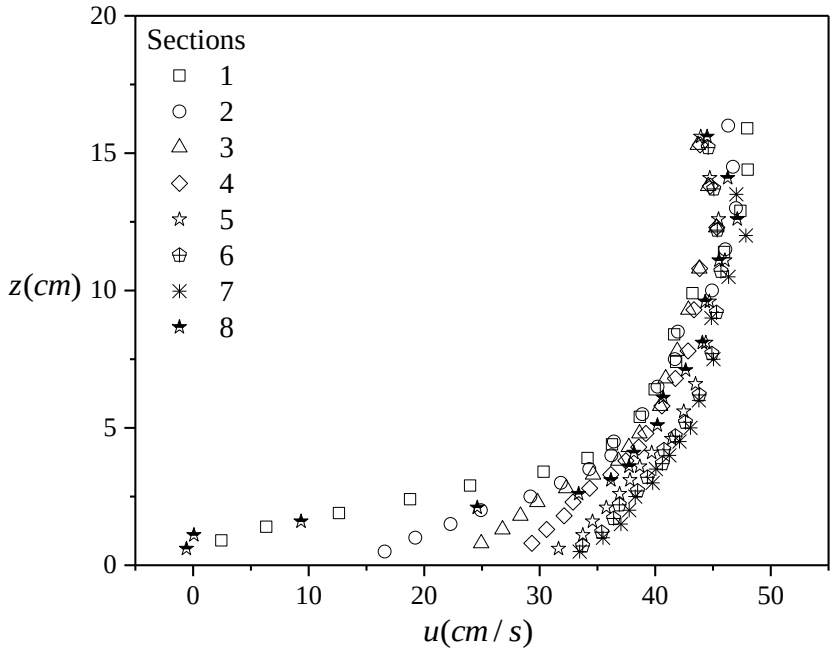

Fig. 2 Streamwise mean velocity profiles u measured over the dune roughened with sediment particles of D_{50} = 0.23 mm in Run D1-0.23

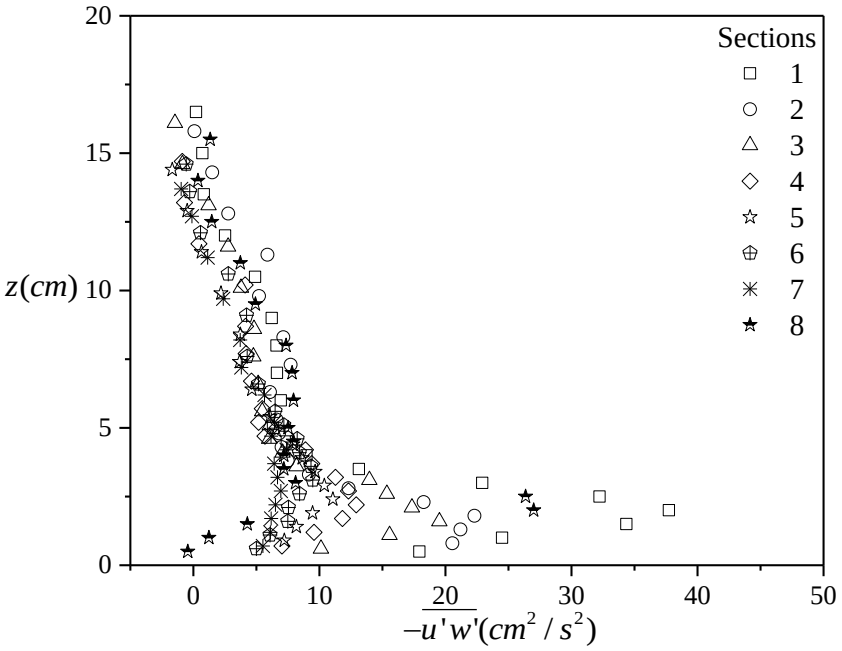

Fig. 3 Reynolds shear stress $-\overline{u'w'}$ profiles measured over the dune roughened with sediment particles of D_{50} = 0.44 mm in Run D2-0.44

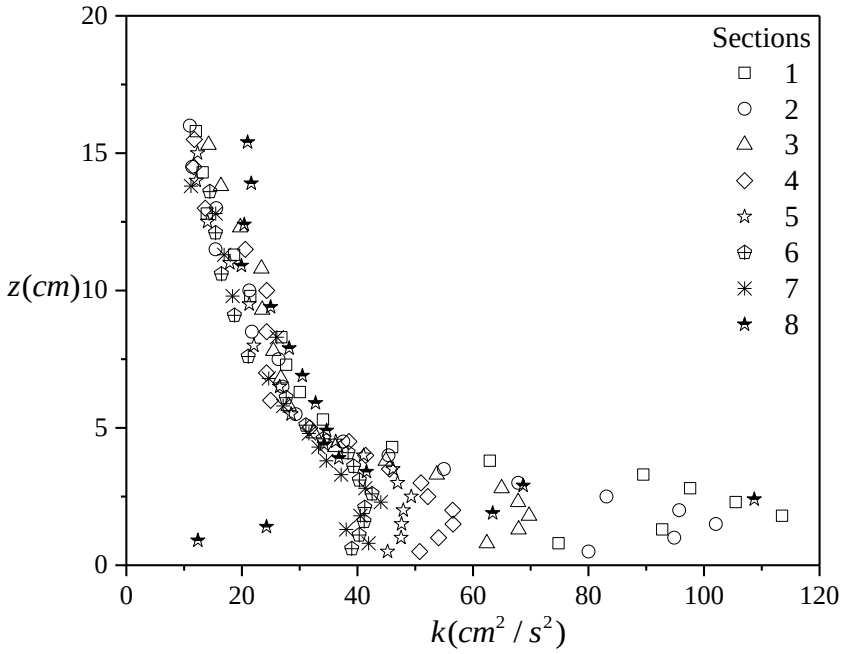

Fig. 4 Turbulent kinetic energy k profiles measured over the dune roughened with sediment particles of D_{50} = 0.86mm in Run D1-0.86

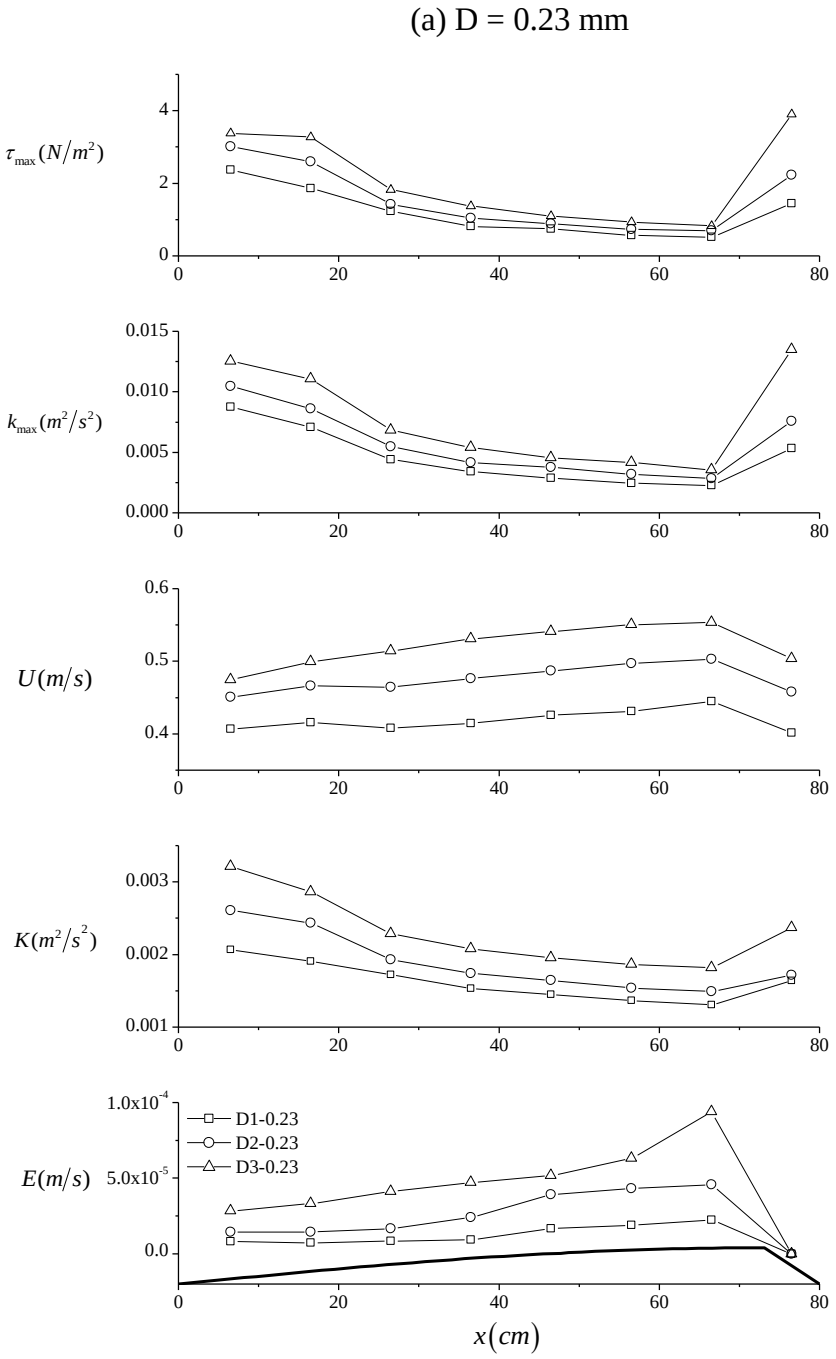

Fig. 5 Variations of near-bed (τ_{max}, k_{max}), depth-averaged flow parameters (U, K) and the pickup rate E over the dune

(b) D = 0.44 mm

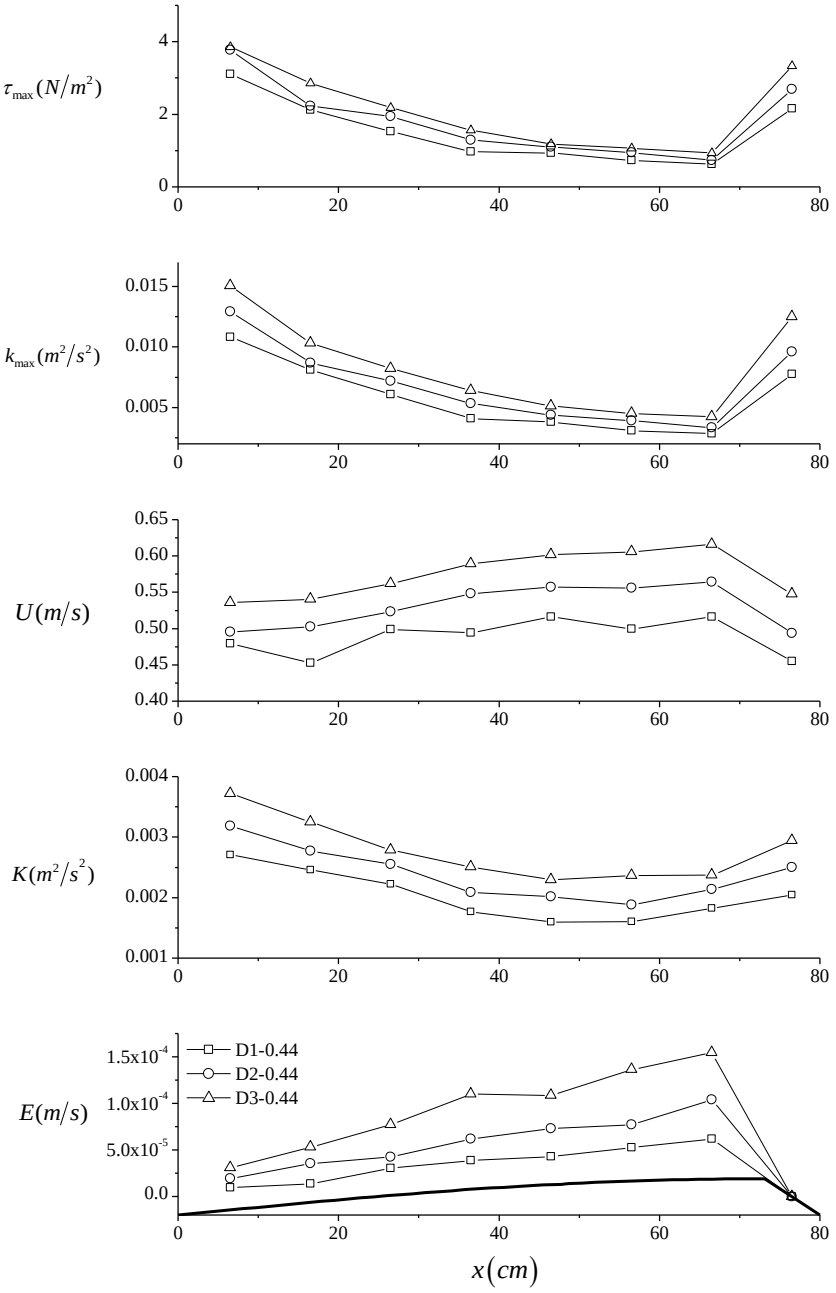

Fig. 5 Continued

(c) D = 0.86 mm

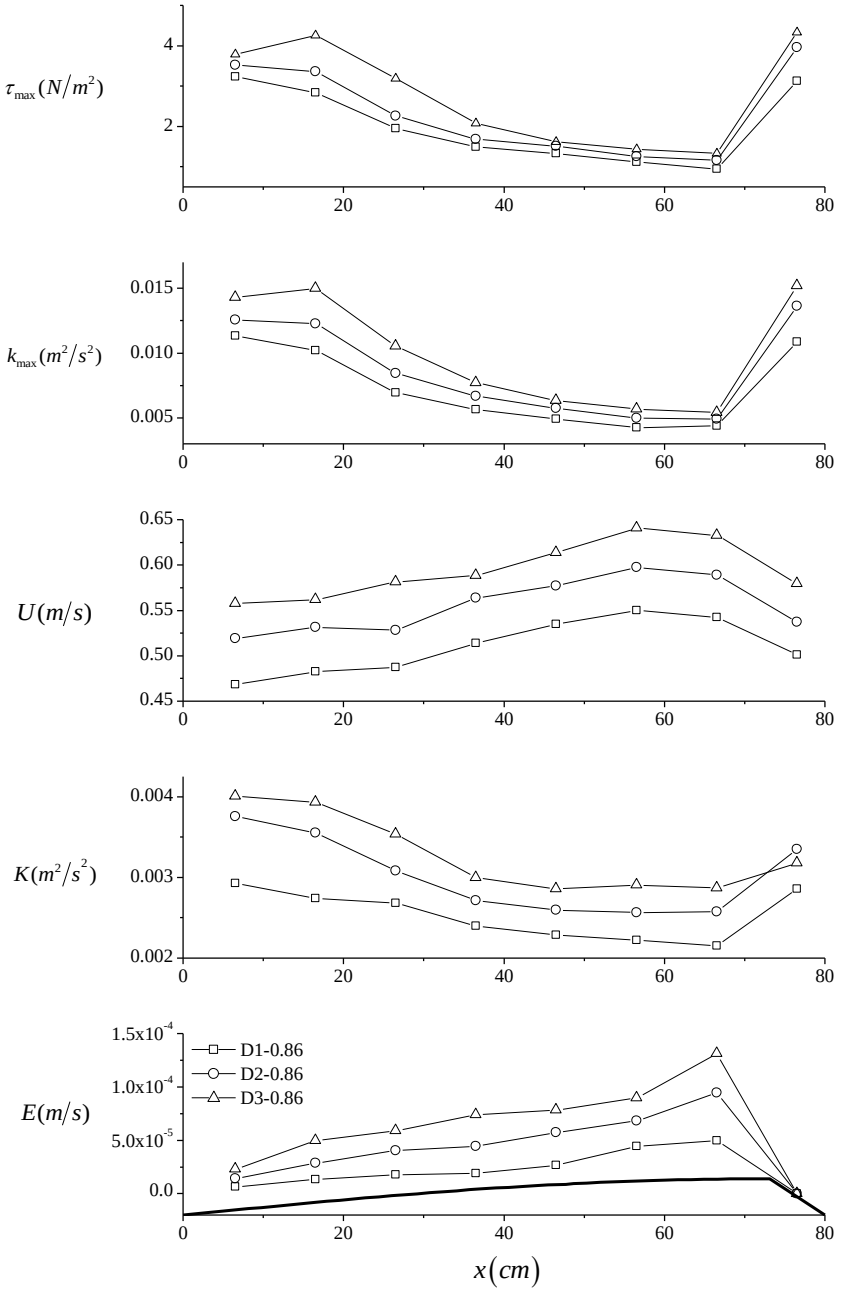

Fig. 5 Continued

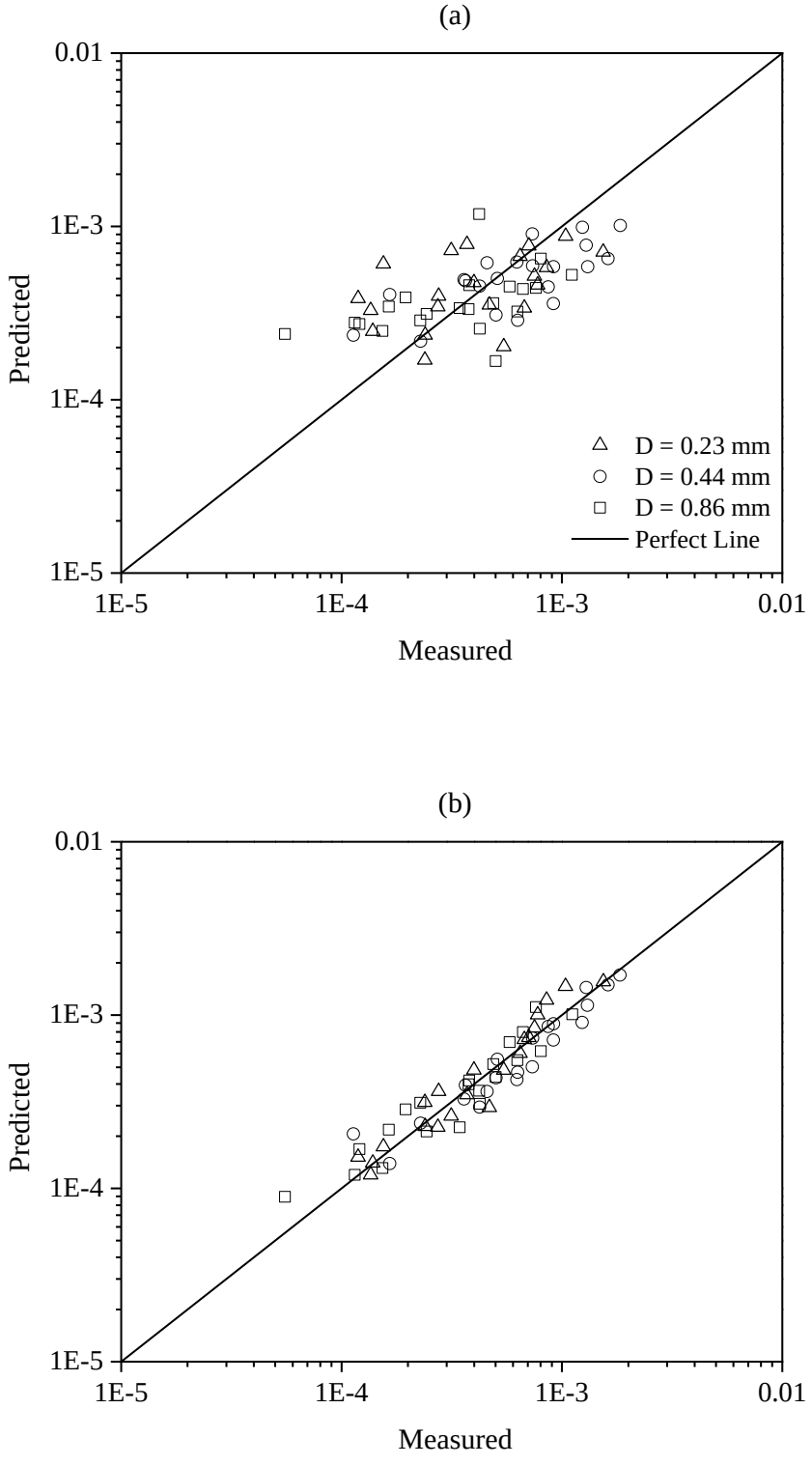

Fig. 6 Comparison of results of E_* obtained using proposed equations: (a) Eq. (6), and (b) Eq. (10)

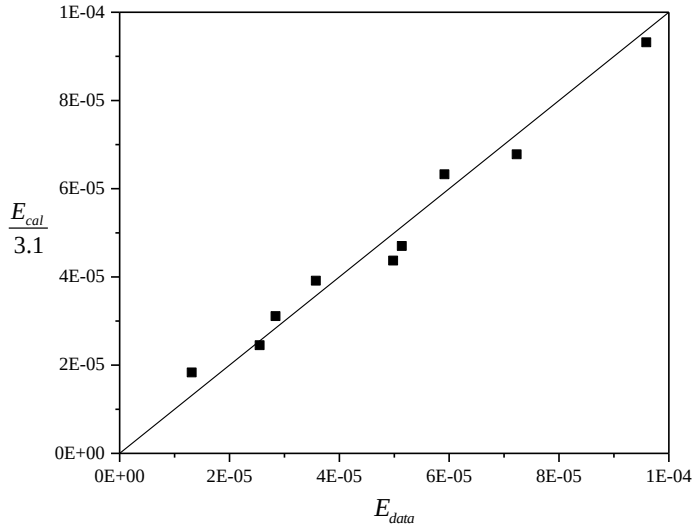

Fig. 7 Comparison of spatial averaged E measured over the dune (E_{data}) and that calculated from Van Rijn's [39] formula Eq. (14) (E_{cal})